Gravitational waves from kinetic preheating

Peter Adshead,[1] John T. Giblin, Jr.,[2,3,4] and Avery Tishue[1]

[1]*Illinois Center for Advanced Studies of the Universe and Department of Physics, University of Illinois at Urbana-Champaign, Urbana, Illinois 61801, USA*

[2]*Department of Physics, Kenyon College, Gambier, Ohio 43022, USA*

[3]*CERCA/ISO and Department of Physics, Case Western Reserve University, Cleveland, Ohio 44106, USA*

[4]*Center for Cosmology and AstroParticle Physics (CCAPP) and Department of Physics, The Ohio State University, Columbus, Ohio 43210, USA*

(Received 1 April 2024; accepted 26 July 2024; published 30 August 2024)

We study gravitational wave production during kinetic preheating after inflation with a focus on scenarios that arise in α-attractor models where a scalar dilatonlike inflaton is kinetically coupled to a second scalar field. We present high-resolution lattice simulations of three α-attractor models for a range of parameters to probe regions where preheating is efficient. We find that preheating in these models can be extremely violent, resulting in gravitational wave energy densities that can be constrained by cosmic microwave background measurements of the effective number of relativistic species, $N_{\rm eff}$.

DOI: 10.1103/PhysRevD.110.043536

I. INTRODUCTION

An early phase of accelerated expansion, inflation [1–5], solves the horizon and flatness problems of the hot big bang cosmology. Quantum vacuum fluctuations of the fields and metric during inflation are stretched outside the horizon before later reentering to seed the density fluctuations that eventually give rise to the inhomogeneities of the cosmic microwave background (CMB) and the large scale structures in the Universe today [6–9]. However, the microphysical origin of the accelerated expansion is far from understood. The simplest models for inflation (for example, Refs. [5,10]) are now strongly disfavored [11,12] and nonminimal inflationary mechanisms (for example, Starobinsky inflation [2], Higgs inflation [13], and α-attractors [14]) are now the leading candidates for the theory of inflation.

An inflationary cosmology consistent with the present observable Universe requires that the energy in the inflaton must have been transferred into matter degrees of freedom to ignite the hot big bang in time for big bang nucleosynthesis [15]—the Universe must be reheated. Yet reheating remains one of the most poorly understood epochs of our cosmic history due to the dearth of observational probes. Because reheating is a local process, the information about its dynamics is largely erased as the standard model plasma reaches local thermal equilibrium. Further, the nonlinear gravitational evolution of structure formation washes out information on scales relevant to preheating. Studies of the physics of preheating with direct observational predictions therefore remain acutely important and timely.

The nonperturbative decay of the inflaton, known as preheating [16–19], often occurs at the end of inflation; the explosive production of particles during this epoch can lead to distinctive gravitational signatures that persist through the opaque, hot, dense phases of early expansion of the Universe. Among these signatures are the production of a high-frequency stochastic gravitational wave background [20–31], and collapsed compact objects such as primordial black holes [32–39] or compact minihalos [40,41]. Nongravitational signatures include the production of primordial magnetic fields [42], and the possible generation of the baryon asymmetry, [43–49]. These signatures may provide important observational evidence of the reheating and post-inflationary epochs and lead to clues about the microphysics of the early Universe.

In this paper, motivated by observationally favored, nonminimal classes of inflationary model involving kinetically coupled scalar fields [50–52], we study a type of kinetic preheating in which the inflaton is coupled to a second scalar field via a dilatonlike interaction [50,53,54]. We specialize to exponential-type couplings that arise in dilaton-axion theories, where the dilaton drives inflation. Generalizing our previous work [54], we explore the effects of different potentials on preheating and study the production of gravitational waves. We characterize the conditions under which the predicted gravitational wave spectra can be constrained by present or next-generation CMB measurements of the effective number of relativistic degrees of freedom, $N_{\rm eff}$. Importantly, the class of models we study here can generically produce gravitational wave backgrounds loud enough that CMB bounds on $N_{\rm eff}$ may

provide constraints on these models. Here, we continue to restrict our attention to scenarios where the axion does not play a role during inflation, and enters the reheating phase with no vacuum expectation value (VEV); this makes this work distinct from other preheating scenarios in α-attractor models, [55–57], which have also been shown to generate gravitational wave backgrounds [58,59].

This paper is organized as follows. In Sec. II we describe the model and derive the equation of motion for the fields and the background Friedmann-Lemaître-Robertson-Walker spacetime. We then analyze the growth of small fluctuations during the coherent oscillations at the end of inflation and validate our code using a Floquet analysis in Sec. III. In Sec. IV we describe the numerical methods we use to study the preheating period, and in Sec. V we discuss our results, in particular characterizing the reheating efficiency and gravitational wave production in the models we study. Our conclusions are presented in Sec. VI.

We use natural units, $\hbar = c = 1$, and define the reduced Planck mass $M_{\rm pl} = 1/\sqrt{8\pi G}$. We use the "mostly plus" metric convention and repeated/contracted Greek spacetime indices are summed via the Einstein summation convention.

II. THE MODEL

We consider a theory with an inflaton, ϕ, and a second scalar field, χ, minimally coupled to Einstein gravity described by the Langrangian,

$$\mathcal{L} = -\frac{M_{\rm Pl}^2}{2}R - \frac{1}{2}(\partial\phi)^2 - \frac{W(\phi)}{2}(\partial\chi)^2 - V(\phi) - \frac{m_\chi^2}{2}\chi^2, \quad (1)$$

where R is the Ricci scalar. The inflaton interacts with χ via an exponential dilatonlike coupling [51,52],

$$W(\phi) = e^{2\phi/\mu}. \quad (2)$$

For this work, we assume that the field χ has no VEV during inflation. Note that this configuration is stable, as shown in Ref. [60].

During inflation, potentials that *plateau*, e.g. polynomial attractors [53] or α-attractors [50], are favored by the CMB [11,12]. Phenomenologically, α-attractors are particularly interesting as, once the normalization of the scalar power spectrum is specified, the single parameter μ that controls the remaining freedom in specifying the potential also controls the kinetic coupling. We consider potentials in this class including the asymmetric E-model α-attractor [50]

$$V = \frac{m^2\mu^2}{2}\left(1 - e^{-\frac{\phi}{\mu}}\right)^2, \quad (3)$$

the symmetric T-model α-attractor

$$V = \frac{m^2\mu^2}{2}\tanh^2\left(\frac{\phi}{\mu}\right), \quad (4)$$

and the polynomial α-attractor [53]

$$V = \frac{m^2\mu^2}{2}\frac{\phi^2}{\phi^2+\mu^2}. \quad (5)$$

Depending on the choice of μ, these potentials lead to different phenomenology at the end of inflation. In the limit where $\mu \gg M_{\rm pl}$, the potential is very well approximated as a quadratic. For smaller values of $\mu \lesssim M_{\rm pl}$, such as those studied in [61], the potential causes anharmonic oscillations of the ϕ field. These anharmonic contributions during preheating generate self-resonances that cause the homogeneous mode of ϕ to decay. In the absence of a coupled field, these anharmonic oscillations have been shown to create oscillons [62–77] and produce gravitational waves [78,79]. While these self-resonances also occur in the model presented here, we demonstrate that the additional instabilities in the axion field can dominate the preheating phase.

The action, Eq. (1), leads to the classical equations of motion for the fields ϕ and χ,

$$\ddot{\phi} = -3\frac{\dot{a}}{a}\dot{\phi} + \frac{\nabla^2\phi}{a^2} - \frac{\partial V}{\partial\phi} + \frac{e^{2\phi/\mu}}{\mu}\left(\dot{\chi}^2 - \frac{(\nabla\chi)^2}{a^2}\right), \quad (6)$$

$$\ddot{\chi} = -3\frac{\dot{a}}{a}\dot{\chi} + \frac{\nabla^2\chi}{a^2} - \frac{1}{e^{2\phi/\mu}}m_\chi^2\chi - \frac{2}{\mu}\left(\dot{\chi}\dot{\phi} - \frac{(\vec{\nabla}\chi)\cdot(\vec{\nabla}\phi)}{a^2}\right). \quad (7)$$

Here and in what follows, an overdot represents a derivative with respect to cosmic time. The expansion of the Universe is given by the Friedmann constraint,

$$H^2 = \frac{1}{3M_{\rm pl}^2}\rho. \quad (8)$$

Here $H = \dot{a}/a$, and $\rho = \rho_\phi + \rho_\chi$, where

$$\rho_\phi = \frac{\dot{\phi}^2 + \frac{(\nabla\phi)^2}{a^2} + \phi^2}{2}, \quad (9)$$

and

$$\rho_\chi = \frac{e^{\frac{2\phi}{\mu}}\left(\dot{\chi}^2 + \frac{(\nabla\chi)^2}{a^2}\right) + m_\chi^2\chi^2}{2}. \quad (10)$$

The energy density of the χ field relative to the total energy density, ρ_χ/ρ, serves as a useful figure of merit to characterize the efficiency of preheating; complete reheating occurs when this ratio approaches unity.

In all three α-attractor models, Eqs. (3)–(5), we are free to chose one parameter, in our case μ. Planck [11] constrains the ratio of the squared Hubble rate, H^2, and the slow-roll parameter, $\epsilon = -\dot{H}/H^2$, via the amplitude of scalar fluctuations,

$$\frac{H_{50}^2}{8\pi M_{\rm pl}^2 \epsilon_{50}} = 2 \times 10^{-9}, \tag{11}$$

which fixes m_ϕ. Here, H_{50} and ϵ_{50} are evaluated 50e-foldings before the end of inflation; these quantities as well as m_ϕ vary from one value of μ [and one choice of $V(\phi)$] to another.

III. STABILITY ANALYSIS

Preheating is defined by the parametric or tachyonic amplification of specific bands of modes (of the inflaton or other matter fields to which it is coupled), generally sourced by the homogeneously oscillating mode of the inflaton. We employ Floquet analysis to identify scales on which instabilities exist in these models. We first linearize the equations to study their stability and predict where the instability bands (in the χ field) might occur. We then explore the stability of the linearized solutions about the homogeneous oscillating inflaton background and compare them to our simulations.

While the linearized analysis makes a number of assumptions—both about the self-interactions of the fields and the expansion of the Universe—it is a way to validate our simulations and to gain intuition for the dependence of preheating on the model parameters. In this section, we restrict attention to the quadratic potential, where the inflaton oscillations are harmonic in Minkowski spacetime.

A. Linearized equations

Ignoring spatial gradients, and neglecting the backreaction of the χ field, the equation of motion for the homogeneous mode of the inflaton is

$$\ddot{\phi} + 3H\dot{\phi} + m_\phi^2 \phi = 0. \tag{12}$$

Assuming that the fluctuations of the χ field are linear perturbations, we can study their independent Fourier modes,

$$\chi(t, \mathbf{x}) = \int \frac{d^3k}{(2\pi)^3} \chi_{\mathbf{k}}(t) e^{i\mathbf{k}\cdot\mathbf{x}}, \tag{13}$$

which are subject to the linearized equation of motion,

$$\ddot{\chi}_{\mathbf{k}} + \left(3\frac{\dot{a}}{a} - \frac{2}{\mu}\dot{\phi}\right)\dot{\chi}_{\mathbf{k}} + \left(\frac{k^2}{a^2} + \frac{m_\chi^2}{e^{2\phi/\mu}}\right)\chi_{\mathbf{k}} = 0. \tag{14}$$

We rescale χ to bring its kinetic term to canonical form,

$$\varphi_{\mathbf{k}} \equiv z\chi_{\mathbf{k}} = a^{3/2}\sqrt{W(\phi)}\chi_{\mathbf{k}}, \tag{15}$$

so that Eq. (14) becomes

$$\ddot{\varphi}_{\mathbf{k}} + \left(\frac{k^2}{a^2} + \frac{m_\chi^2}{e^{2\phi/\mu}} - \frac{\ddot{z}}{z}\right)\varphi_{\mathbf{k}} = 0. \tag{16}$$

Substituting $W(\phi) = e^{2\phi/\mu}$, we can evaluate

$$\frac{\ddot{z}}{z} = \left(\frac{3}{2}H + \frac{\dot{\phi}}{\mu}\right)^2 + \left(\frac{3}{2}\dot{H} + \frac{\ddot{\phi}}{\mu}\right). \tag{17}$$

The analogous, linearized equation of motion for the modes of the canonically normalized inflaton, $\pi_{\mathbf{k}} \equiv a^{3/2}\phi_{\mathbf{k}}$, reads

$$\ddot{\pi}_{\mathbf{k}} + \left(\frac{k^2}{a^2} + \frac{\partial^2 V}{\partial\phi^2} - \frac{9}{4}H^2 - \frac{3}{2}\dot{H}\right)\pi_{\mathbf{k}} = 0. \tag{18}$$

We use Eq. (18) to set initial conditions for the fluctuations of the inflaton in our simulations.

B. Floquet analysis

We begin by studying the behavior of Eqs. (12) and (16) in Minkowski space, which can be done analytically. In this limit, $a = 1$ and $H = \dot{H} = 0$, and hence the solution for the homogeneous inflation field is

$$\phi = \phi_0 \cos(m_\phi t). \tag{19}$$

Under these assumptions, the equation of motion for the modes of φ is

$$\ddot{\varphi}_{\mathbf{k}} + \left(\frac{k^2}{a^2} + m_\chi^2 e^{-2\phi/\mu} - \left(\frac{\dot{\phi}}{\mu}\right)^2 - \frac{\ddot{\phi}}{\mu}\right)\varphi_{\mathbf{k}} = 0, \tag{20}$$

which is the equation for a harmonic oscillator with a time-dependent (periodic) effective mass. Floquet's theorem states that solutions to Eq. (20) are of the form $\varphi_{\mathbf{k}} \propto P_+(t)e^{\mu_f t} + P_-(t)e^{-\mu_f t}$, where μ_f is the Floquet exponent and $P_\pm(t) = P_\pm(t+T)$ is a periodic function with period T which is the same period as the time-dependent mass. When $\Re(\mu) \neq 0$, the modes, $\varphi_{\mathbf{k}}$, grow exponentially.

In the small amplitude limit, $\phi_0 \ll \mu$, Eq. (20) can be recast as the Mathieu equation,

$$\frac{d^2\varphi_k}{dz^2} + [p - 2q\cos(2z)]\varphi_k = 0, \tag{21}$$

where $z = m_\phi/2$ and we have defined

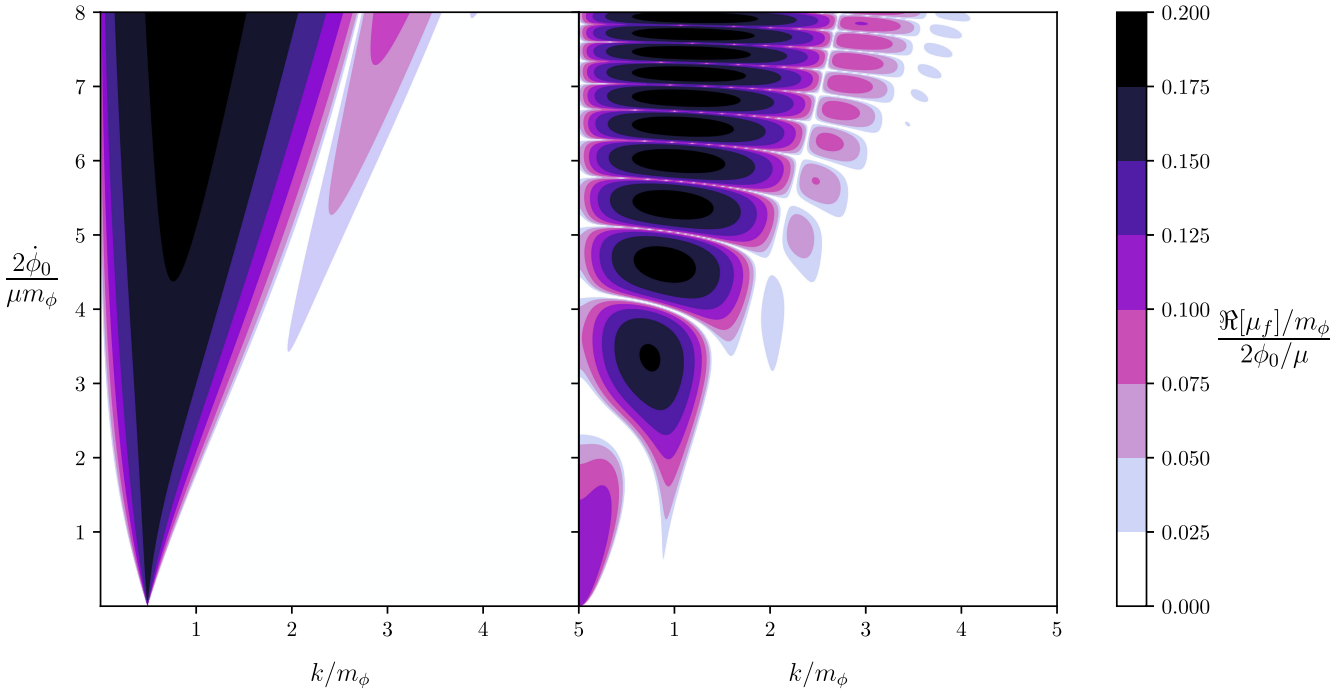

FIG. 1. Contours of the real part of the Floquet exponent showing the regions of parameter space where the modes grow exponentially in the case where χ is massless (left) and massive (right). The parameter space corresponding to exponentially growing modes is significantly different in the two cases, and importantly, for a massive χ field there exists parameter space for exponential growth for modes of arbitrarily long wavelength, even for very small values of $\dot{\phi}_0/\mu m_\phi$. The wave numbers on the horizontal axis correspond to *physical* wave numbers since this analysis assumes a Minkowski spacetime.

$$p = \left(\frac{2k}{m_\phi}\right)^2 + \left(\frac{2m_\chi}{m_\phi}\right)^2, \tag{22}$$

$$q = \frac{2\phi_0}{M}\frac{m_\chi^2}{m_\phi^2}\left(1 - \frac{m_\phi^2}{2m_\chi^2}\right). \tag{23}$$

When $\phi_0 \ll \mu$, $q \ll 1$, the solutions of the Mathieu equation are known to be unstable when $p = n^2$ for $n \in \mathbf{Z}$. Notice that, for $k \ll m_\phi$, if $m_\chi = nm_\phi/2$, then the instability band persists down to arbitrarily small wave numbers; this can also be seen in the right panel of Fig. 1 when directly using Eq. (20). This effect is analogous to that which occurs for kinetically coupled massive vector fields [80].

Floquet exponents can be obtained analytically for small q, and for $m_\chi = m_\phi/2$ they are given by

$$\Re[\mu] = \frac{\phi_0}{\mu}\frac{m_\phi}{4}. \tag{24}$$

Away from this limit, for both large q and $m_\chi \neq m_\phi/2$, the Floquet exponents must be found numerically. These are displayed in Fig. 1, which shows the Floquet exponents, μ_f, as the amplitude of the velocity of the homogeneous mode, $\dot{\phi}_0 = m_\phi\phi_0$, is varied relative to the kinetic coupling, μ, for a set of wave numbers using Eq. (20).

IV. NUMERICAL PROCEDURE

We employ GABE [81] to carry out $3+1$ simulations of the fields ϕ and χ in a self-consistent, but rigidly expanding background (we ignore local gravity). To set our initial conditions, we evolve the equations of motion in the homogeneous limit, Eq. (6) alongside the Friedmann constraint, Eq. (8) for at least $60e$-folds of inflation. This ensures that the system is following the corresponding attractor solution for each model we study. From this homogeneous evolution, we extract ϵ_{50} and H_{50} which allow us to calculate m_ϕ for every choice of potential and μ. These also give the inflaton amplitude and velocity half an e-folding before the end of inflation (inflation ends, by definition, when $\ddot{a} = 0$). We initialize the fluctuations of the inflaton and χ fields from the Bunch-Davies vacuum,

$$\langle|\phi(k)|^2\rangle = (2a\omega_\phi)^{-1}, \tag{25}$$

$$\langle|\chi(k)|^2\rangle = (2a\omega_\chi W(\bar{\phi}))^{-1}, \tag{26}$$

where for each field $\omega = \sqrt{(k/a)^2 + m_{\rm eff}^2}$ and the effective mass squared for ϕ and χ are calculated from the equations of motion Eqs. (18) and (15), evaluated half an e-folding before the end of inflation. Note the factor of W in the χ initial spectrum is a consequence of the fact the kinetic term for χ carries the dilatonlike coupling W.

We start the runs at half an e-folding before the end of inflation to ensure that the effective mass of ϕ is positive, and the modes of interest are in the Bunch-Davies vacuum. We initialize our box to have size $L = H_{\rm end}^{-1} e^{-0.5}$, where $H_{\rm end}$ is the Hubble scale at the end of inflation. This initialization ensures that our box is the size of the horizon at the end of inflation and the onset of preheating. These initial conditions seed the fully nonlinear evolution of the system Eqs. (6) and (7) alongside the homogenous expansion of the Universe, . (8), from half an e-folding before the end of inflation through the reheating epoch. Unless otherwise noted, we use grids with $N^3 = 256^3$ points with periodic boundary conditions. We set the time step is set to be $\Delta t = L/N/30 < L/N/\sqrt{3}$ to satisfy the Courant-Friedrichs-Lewy condition.

A. Instability in a toy model

Before we turn to the α-attractor models, we validate our simulations using the quadratic potential,

$$V(\phi) = \frac{1}{2} m^2 \phi^2, \tag{27}$$

where we set $m_\phi = 5 \times 10^{-5} M_{\rm pl}$ as a reference value, and compare our full nonlinear results to the linearized Floquet analysis from Sec. III above. In practice m_ϕ sets the scale of the simulation and is only relevant for setting the initial conditions of the fields. In Minkowski space, a quadratic potential leads to a harmonic oscillation of the homogeneous value of ϕ. While this is not true in an expanding universe, when the ϕ field crosses zero—the point at which particle creation is most violent—we can instantaneously approximate the magnitude of the sinusoidal oscillation to the velocity of the field at the zero crossing, $\phi_0 = \dot{\phi}_0/m_\phi$. Then we can use this value to predict where the instability bands are. We perform a set of simulations where $m_\chi = 0$ and $m_\chi = m_\phi/2$ for a range of μ.

For these runs we are able to start at the end of inflation with an initial comoving box size of $L = 12 m_\phi^{-1} \approx 6 H_{\rm end}^{-1}$ since the quadratic potential prevents tachyonic modes at the end of inflation. In this toy model, we can also take coarser resolution, where $N^3 = 128^3$, which roughly probes modes between $k_{\rm min} = 2\pi/L \approx 0.5 m_\phi$ and the 3D Nyquist fruency, $k_{\rm max} = (128\sqrt{3}/2) k_{\rm min} = 58 m_\phi$. Figure 2 shows the comparison between the Floquet analysis for the first zero-crossing of the homogeneous mode of ϕ and the

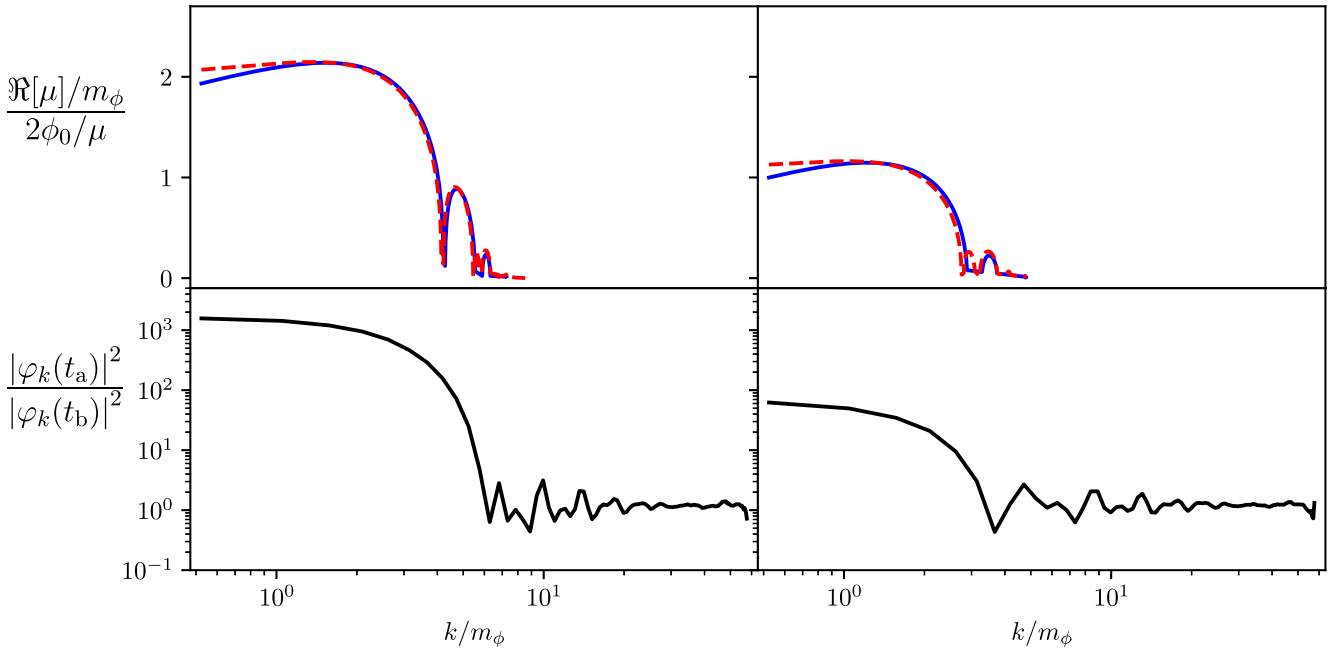

FIG. 2. A comparison of Floquet analysis and mode amplification. The top panels show the Floquet exponent, μ, as calculated from s. (16) (red, dashed) and (20) (blue, solid); curves terminate when the Floquet exponent is identically zero. The bottom panel shows the amplification of the power spectrum of our simulations, $|\varphi_k|^2$, evaluated just before the first zero crossing of the homogeneous mode of ϕ, $t_{\rm b}$, and just after, $t_{\rm a}$. The time interval is symmetric about the zero crossing with width $t_{\rm a} - t_{\rm b} \approx m_\phi^{-1}$. We compare these for two different scenarios; the left panels show the case where $\mu \approx 0.122 M_{\rm pl}$ (corresponding to $2\dot{\phi}/\mu m_\phi \approx 7.92$ during the first zero crossing) and the right panel shows the case where $\mu \approx 0.217 M_{\rm pl}$ (corresponding to $2\dot{\phi}/\mu m_\phi \approx 4.46$ during the first zero crossing). Note that the relative amplitude and the range of k-modes that are amplified show agreement with Fig. 1.

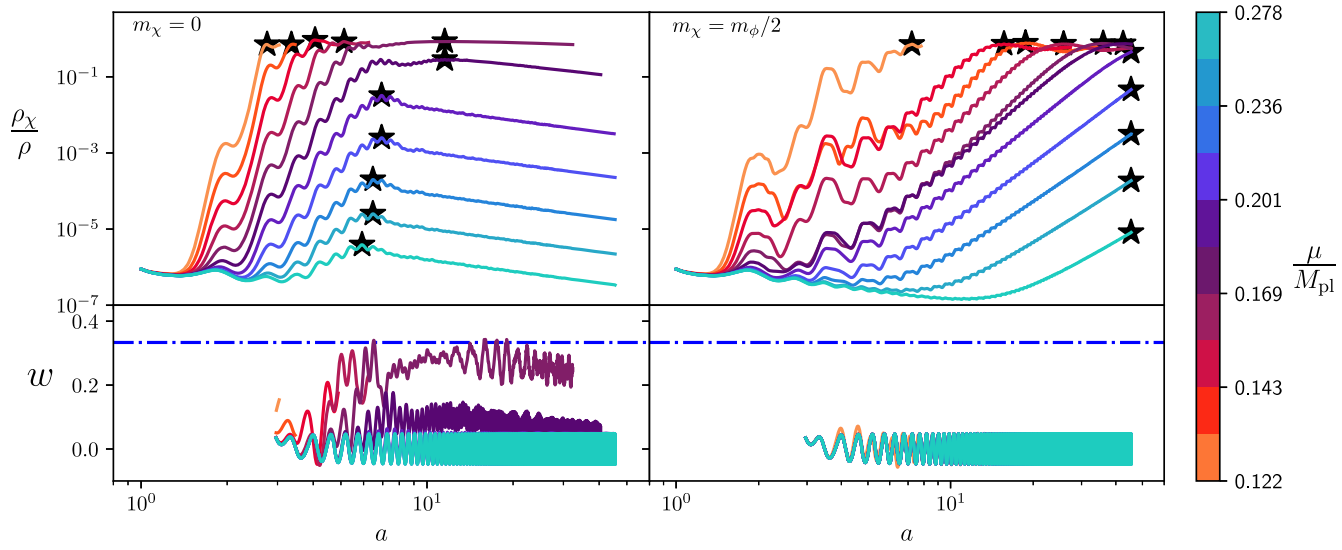

FIG. 3. Reheating efficiency for the toy-model given by Eq. (27) for a range of μ values as a function of e-folding in the case where χ is massless (top left) and massive, $m_\chi = m_\phi/2$ (top right) and the equation of state for both cases, $m_\chi = 0$ (bottom left) and $m_\chi = m_\phi/2$ (bottom right), time-averaged over a period of the homogeneous mode of ϕ. The horizontal (blue, dot-dashed) line corresponds to a pure radiation-dominated equation of state, $w = 1/3$. Smaller μ values correspond to a larger dilatonlike couplings W, yielding more efficient reheating. Warm colors (cool colors) correspond to the data produced by simulations with a smaller (larger) μ values, as indicated by the colorbar. The stars represent the points in each run where the ratio ρ_χ/ρ is largest. Reheating into the χ field is faster and more complete for smaller μ values.

results of two fully nonlinear simulations, one with $\mu = 0.122 M_{\rm pl}$ and one with $\mu = 0.217 M_{\rm pl}$, both in the case where $m_\chi = 0$. We see excellent agreement with regards to which modes are amplified and the relative strength of these amplifications. Note that the results of the nonlinear simulations do not show all the bumps of the Floquet analysis; this is due to the fact that the modes from the nonlinear simulations are binned and that, even over the short timescale over which we compare, the physical size of the modes vary enough to smear out the finest features of the Floquet analysis. Nonetheless, this agreement validates that kinetic preheating is responsible for the particle creation in these models.

We also calculate the efficiency of preheating in this toy model. Figure 3 shows the ratio of energy in the χ field compared to the total energy in the box as a function of scale factor throughout the simulation for a range of values of μ for both $m_\chi = 0$ and $m_\chi = m_\phi/2$. While we terminate all the runs when the scale factor hits $a \sim 500$, we see that when χ is massive, the low-k instability continues to source particle creation until we end the simulation. In the Appendix, we compute the spectrum of gravitational waves from these toy scenarios.

V. RESULTS

In this section, we present the results of our nonlinear simulations. We demonstrate that kinetic preheating can be extremely efficient in α-attractor models, across all variants of the potential we study. We also compute the resulting spectrum of gravitational waves, and demonstrate that current and upcoming CMB measurements will constrain kinetic preheating in these models.

A. Preheating

We begin by examining the reheating efficiency in the three α-attractor models from Sec. II. Figure 4 shows the ratio ρ_χ/ρ as a function of e-folding number for a range of μ values for the E-model, P-model, and T-model in the left, center, and right panels, respectively. In all models preheating is more efficient as μ is decreased. For a fixed μ value, we find that reheating is most (least) efficient for the T-model (E-model). This can be seen more clearly in Fig. 5, where we show the maximum energy density ratio ρ_χ/ρ achieved in each simulation as a function of μ. Generally, for each model there is a sharp transition between inefficient ($\rho_\chi/\rho \ll 1$) reheating and complete reheating $\rho_\chi/\rho \sim 1$ that occurs when μ drops below a critical value. This transition occurs at larger μ values for the T-model and lower values for the E-model, and beyond this transition all three models reach roughly the same maximum value of ρ_χ/ρ. Finally, for each model, our results demonstrate that if μ is small enough, preheating proceeds very rapidly and violently, causing the simulations to crash before reheating can fully complete (see the cool colored curves that end abruptly in Fig. 4). This is a physical consequence of the fact that the kinetic coupling W generates an infinite sequence of higher-dimensional operators. These operators generate a high-frequency, ultraviolet cascade that quickly

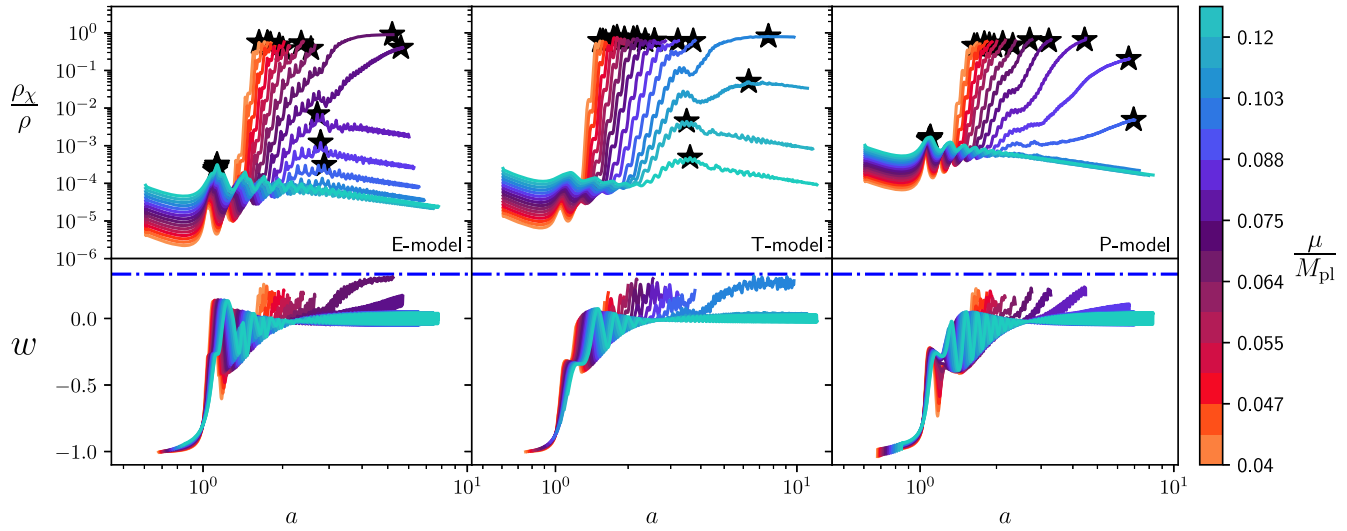

FIG. 4. Reheating efficiency, ρ_χ/ρ, for the E-model (top left), T-model (top center) and P-model (top right) α-attractor given by Eqs. (3)–(5) for a range of μ values as a function of e-folding and the equation of state for each scenario, E-model (bottom left), T-model (bottom center), and P-model (bottom right), time-averaged over a period of the homogeneous mode of ϕ. The horizontal (blue, dot-dashed) line corresponds to a pure radiation-dominated equation of state, $w = 1/3$. Smaller μ values correspond to a larger dilatonlike couplings W [and a broader potential $V(\phi)$], yielding more efficient reheating. Warm colors (cool colors) correspond to the data produced by simulations with a smaller (larger) μ values, as indicated by the colorbar. The stars represent the points in each run where the ratio ρ_χ/ρ is largest.

transfers power to high-frequency modes that our simulations cannot resolve [82,83].

B. Gravitational waves

Strong resonance dynamics during preheating generically leads to the robust generation of gravitational waves [20–31]. The α-attractor models studied here can lead to very efficient kinetic preheating and we anticipate that they

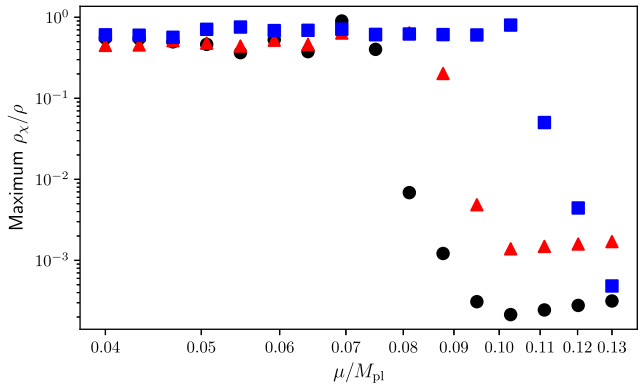

FIG. 5. Comparison of maximum ratio of energy densities ρ_χ/ρ between the three different α-attractor models, the E-model (black, circles), T-model (blue, squares), and P-model (red, triangles) over a range of μ values, demonstrating the critical μ value for which reheating becomes efficient in each model. These are the maxima that correspond to the starred points in Fig. 4. The E-model generally requires the smallest μ value to reheat efficiently; by contrast, the T-model can reheat efficiently at larger μ values.

may also lead to a strong gravitational wave background. Here, we calculate the power in gravitational waves by passively calculating tensor perturbations of the metric, following the basic procedure of [24]. Ignoring scalar and vector perturbations, the metric reads

$$ds^2 = -dt^2 + a^2(\delta_{ij} + h_{ij}^{\rm TT})dx^i dx^j. \tag{28}$$

Here, the transverse-traceless perturbations of the spatial metric, $h_{ij}^{\rm TT}$, are gravitational waves. These satisfy the linearized equation of motion,

$$\Box h_{ij}^{\rm TT} = 16\pi G T_{ij}^{\rm TT}, \tag{29}$$

which follows from the Einstein equation. Gravitational waves are sourced by the transverse-traceless projection of the anisotropic stress tensor,

$$T_{ij}^{\rm TT} = \left(P_{il}P_{jm} - \frac{1}{2}P_{ij}P_{lm}\right)T_{lm}, \tag{30}$$

where P is the projection operator,

$$P_{ij} = \delta_{ij} - \frac{k_i k_j}{k^2}. \tag{31}$$

Equation (29) allows us to compute the evolution of h_{ij}, from which we can compute the effective stress energy tensor for gravitational waves [84],

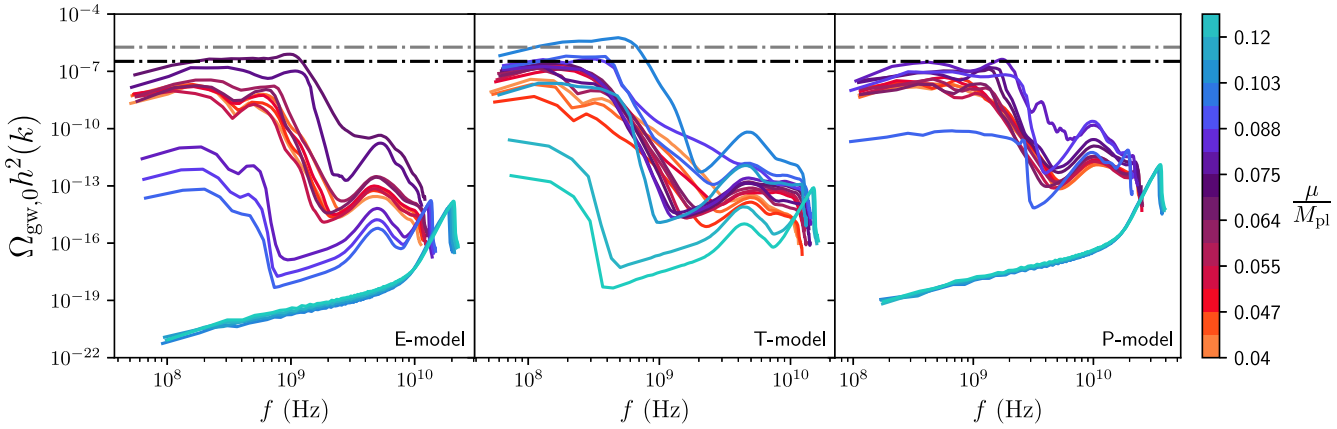

FIG. 6. The gravitational wave spectral energy density for the E-model (left), T-model (center), and T-model (right) α-attractor kinetic reheating scenarios for a range of μ values. These spectra are evaluated at the starred-locations in Fig. 4. Simulations that reheat completely and last longer produce stronger gravitational wave backgrounds that are particularly enhanced at the low frequency end of the resolved spectrum. The dot-dashed lines show the 2σ constraints on the amplitude of the gravitational wave spectrum that can be inferred from current (Planck [86], gray) and future (CMB-S4 [87], black) CMB measurements of $N_{\rm eff}$. The smaller, high-frequency peaks in these spectra are a numerical artifact.

$$T^{\rm gw}_{\mu\nu} = 8\pi G\langle h^{\rm TT}_{ij,\mu} h^{ij}{}_{,\nu}{}^{\rm TT}\rangle. \tag{32}$$

The energy density in gravitational waves is therefore

$$\rho_{\rm gw} = 8\pi G|h^{\rm TT}_{ij,0}|^2, \tag{33}$$

and the spectral energy density of the gravitational waves during the simulation is found from

$$\Omega_{\rm gw}(k) \equiv \frac{1}{\rho}\frac{d\rho_{\rm gw}}{d\ln k} = \frac{1}{24\pi^2 L^3}\frac{k^3}{H^2}\sum_{i,j}|\dot{h}_{ij}(k,t)|^2. \tag{34}$$

To compare between simulations, we evaluate the gravitational wave spectra when ρ_χ/ρ is at its maximum. This occurs at the points identified with stars in Fig. 4. Once computed, the spectral energy density in gravitational waves today can be found from [21,22]

$$\Omega_{\rm gw,0}h^2 = \Omega_{\rm rad,0}h^2\frac{g_\star(a_{\rm r})}{g_\star(a_0)}\left(\frac{g_{\star S}(a_{\rm r})}{g_{\star S}(a_0)}\right)^{-4/3}\Omega_{\rm gw}(a), \tag{35}$$

with frequencies today given by

$$f = \frac{k/2\pi a}{\rho(a)^{1/4}}\rho_{\rm rad}(a_0)^{1/4}\left(\frac{g_\star(a_{\rm r})}{g_\star(a_0)}\right)^{1/4}\left(\frac{g_{\star S}(a_{\rm r})}{g_{\star S}(a_0)}\right)^{-1/3} \tag{36}$$

$$\approx 3.2\times 10^{10}\ {\rm Hz}\frac{k/a}{\sqrt{H(a)M_{\rm pl}}}\left(\frac{g_\star(a_{\rm r})/g_\star(a_0)}{100}\right)^{-1/12}. \tag{37}$$

In the preceding expressions $g_\star$ is the number of ultrarelativistic degrees of freedom evaluated at reheating, a_r, or today, a_0, $g_\star(a_{\rm r})/g_\star(a_0) \approx 100$. We also make the standard assumption that the Universe is radiation-dominated at the time when the power spectrum in the simulation is evaluated.[1] We examine the validity of this assumption explicitly by evaluating the equation of state, $w = \langle p\rangle/\langle\rho\rangle$, averaged over one period of the homogeneous mode of ϕ, in each of our simulations. The bottom panels of Figs. 3 and 4 show that the equation of state generally approaches $w = 1/3$ in cases where the decay field is massless and preheating is efficient. For many of these cases, the equation of state does not fully reach $w = 1/3$ if the simulation ends due to an ultraviolet cascade. We also note that we are limited in the range of frequencies for which we can compute the gravitational wave spectra, bounded below by the size of the box and bounded above by the Nyquist frequency of the grid. Nevertheless, we are able to resolve the gravitational wave spectra over several decades in frequency around 10^{10} Hz, as indicated by Eq. (37).

We present the gravitational wave spectra from preheating in the three α-attractor scenarios over a range of μ values in Fig. 6. The spectra in each model share some similarities, but in general the spectra depend nontrivially on μ. Roughly speaking, the gravitational wave spectra are strongest (that is, they reach a largest maximum value at some f) for values of μ near the critical value (the largest value of μ for which a model preheats). For these values, the physics of reheating is sufficiently violent to produce a strong gravitational wave spectrum, but the process also

[1]Note that, the transfer functions in Eq. (35) assume continuous radiation domination from the time of gravitational wave emission until matter-radiation equality at redshift $z \sim 3000$. However, in cases where the equation of state deviates from $w = 1/3$ due to the domination of some exotic species, these transfer functions are modified.

persists for longer, and the combination of these two factors leads to the strongest gravitational wave spectra [85].

For models where μ at and below the critical value necessary for complete reheating, reheating is very fast and the simulations end very quickly as described in Sec. V A, yielding somewhat weaker gravitational wave spectral energy density, with similar spectral shapes. We note that the ultraviolet cascade in the field sector makes evolving the simulations any further prohibitive in our setup; more sophisticated numerical techniques, larger grids, and longer run times might be able to resolve preheating in these models. The gravitational wave spectra we evaluate in these scenarios are likely lower bounds on the actual generated spectra.

Importantly, in all three α-attractor models, the gravitational wave spectra can reach $\Omega_{\mathrm{gw},0} \approx 10^{-6} - 10^{-7}$ over a range of scales. A gravitational wave background of this strength contributes significantly to the radiation content of the early Universe and can therefore potentially be constrained by bounds on extra relativistic degrees of freedom, $\Delta N_{\mathrm{eff}} = N_{\mathrm{eff}} - 3.044$ [88–90]. If we take the conservative simplifying assumption there are no additional ultrarelativistic degrees of freedom at recombination beyond the Standard Model and the gravitational waves from preheating, then the present-day gravitational wave energy density is related to the present day photon energy density and ΔN_{eff} via

$$\Omega_{\mathrm{gw},0}h^2 = \Omega_{\gamma,0}h^2 \frac{7}{8}\left(\frac{4}{11}\right)^{4/3} \Delta N_{\mathrm{eff}}, \tag{38}$$

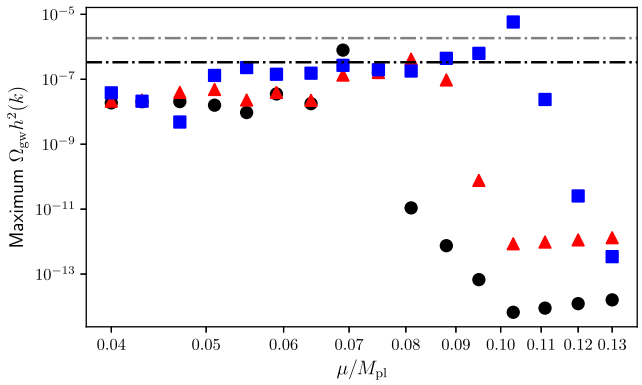

FIG. 7. The maximum gravitational wave spectral energy density from kinetic preheating for each α-attractor model, the E-model (black, circles), T-model (blue, squares), and P-model (red, triangles) over a range of μ values. Each point represents the maximum value of the gravitational wave spectra presented in Fig. 6. The gravitational wave background is significantly stronger for models that completely reheat. The dot-dashed lines show the 2σ constraints on the amplitude of the gravitational wave spectrum that can be inferred from current (Planck [86], gray) and future (CMB-S4 [87], black) CMB measurements of N_{eff}.

where the present-day photon energy density is $\Omega_{\gamma,0}h^2 \approx 2.47 \times 10^{-5}$. Planck 2018 [11] gives an upper bound of $|\Delta N_{\mathrm{eff}}| < 0.33$ (95% CL) which yields a constraint on the gravitational wave energy density $\Omega_{\mathrm{gw},0}h^2 \lesssim 1.851 \times 10^{-6}$. A joint BBN-CMB analysis [91] gives a slightly stronger bound $|\Delta N_{\mathrm{eff}}| < 0.168$ (95% CL), which tightens the constraint to $\Omega_{\mathrm{gw},0}h^2 \lesssim 9.424 \times 10^{-7}$. This means that under the assumptions listed here, and depending on the value of μ, these models can already be constrained at the 2σ level as a consequence of violent gravitational wave production during the preheating epoch. This picture is even more promising when looking ahead to next generation CMB experiments; the projected sensitivity of CMB-S4 is $|\Delta N_{\mathrm{eff}}| < 0.06$ (95% CL) [87], which further tightens the constraint on the gravitational wave spectrum to $\Omega_{\mathrm{gw},0}h^2 \lesssim 3.366 \times 10^{-7}$. In Fig. 7, we show the maximum energy density in gravitational waves for each α-attractor model over a range of μ values as well as the CMB bound from Planck and projected bound from CMB-S4. This indicates that several μ values are already in 2σ tension with bounds on ΔN_{eff}, emphasizing the role that next-generation CMB experiments will play in constraining the parameter space in these models as a consequence of gravitational waves production during the violent preheating epoch.

VI. DISCUSSION AND CONCLUSIONS

In this paper we have studied gravitational wave production from kinetic preheating after inflation in α-attractor potentials. These nonminimal inflationary models are currently among the leading candidates for the theory of inflation. In these models, one or more scalar fields are nonminimally coupled to the Ricci scalar. After transforming to the Einstein frame and canonically normalizing the inflaton, these models generically lead to exponential couplings between the inflaton and any other degree of freedom in the theory. Motivated by these models, in this work we have investigated the effect of an exponential kinetic coupling between the inflaton and an ultralight spectator field during the onset of reheating after α-attractor inflation.

Beyond their appeal as inflationary candidates, α-attractor models also have the attractive feature that they effectively contain only one free parameter. This parameter characterizes both the shape of the inflationary potential as well as the strength of the couplings of the inflaton to other degrees of freedom. After the normalization of the scalar power spectrum is fixed, the remaining free parameter sets the tensor-to-scalar ratio. In this paper we have extended the study of these models to the preheating phase, characterizing the conditions under which these models can efficiently preheat the Universe and produce strong gravitational wave backgrounds.

Our analysis has shown that kinetic preheating in the three classes of α-attractor potentials studied here can be

very efficient and is highly sensitive to the sole free parameter μ. For normalization of the scalar spectrum fixed to the observed value, complete reheating is achieved for $\mu/M_{\rm pl} \lesssim 0.077$ or the E-model, Eq. (3), $\mu/M_{\rm pl} \lesssim 0.11$ for the T-model, Eq. (4), and $\mu/M_{\rm pl} \lesssim 0.81$ for the P-model, Eq. (5). Because of the exponential sensitivity of the kinetic coupling to μ, even slightly smaller values of μ yield significantly faster preheating. That is, there exists an upper bound on μ below which both the inflationary predictions agree with the CMB and the kinetic preheating is highly efficient.

We have shown that highly efficient preheating in these models leads to the creation of a gravitational wave background from the preheating phase, with an amplitude and spectral energy density that far exceeds the stochastic inflationary background in the same frequency band. This frequency band is well above the range probed by both current and next generation direct detectors such as the Advanced Laser Interferometer Gravitational-Wave Observatory [92], the Laser Interferometer Space Antenna [93], Cosmic Explorer [94], and the Einstein Telescope [95]. However, we have demonstrated that in some cases, these backgrounds are strong enough to be constrained at the 2σ level by present and next-generation CMB bounds on $N_{\rm eff}$. Kinetic-preheating in α-attractor scenarios is therefore both a highly predictive and also falsifiable theory of the primordial Universe, which is desirable given the challenge of constructing concrete early Universe models that connect with present or near-term observations.

The present work suggests several promising avenues for further investigation into kinetic preheating. For example, while our analysis has demonstrated intense gravitational wave production, further work is needed to understand the full gravitational dynamics in these scenarios. In particular, we plan to investigate the fully nonlinear gravitational dynamics by implementing full general relativity in the simulations to study the potential for the production of primordial black holes and other compact objects [96–98].

ACKNOWLEDGMENTS

We thank Mustafa Amin and Zachary Weiner for early conversations regarding kinetic couplings. We thank Reid Pfaltzgraff-Carlson for early collaboration on this project. P. A. and A. J. T. are supported in part by the United States Department of Energy (No. DE-SC0015655). J. T. G. is supported in part by the National Science Foundation, (No. PHY-2309919). The authors gratefully acknowledge support from the Simons Center for Geometry and Physics, Stony Brook University at which some of the research for this paper was performed. P. A. and J. T. G. thank the Yukawa Institute for Theoretical Physics at Kyoto University, where some of this work was completed during the YITP-T-23-02 on "Cosmology and Gravity 2024." Simulations were performed using the Ohio supercomputer center [99] as well as on hardware provided by the National Science Foundation, Kenyon College.

APPENDIX: GRAVITATIONAL WAVES FROM A TOY MODEL

For completeness, in this appendix we compute the gravitational wave spectra from the toy model in Sec. IV A where the inflationary potential is quadratic. In this model, the presence of a nonzero mass in the χ field only slightly changes the value of the kinetic coupling, μ, required to fully preheat. Figure 8 shows that, independent of our two choices for m_χ, $\mu \lesssim 0.18 M_{\rm pl}$ yields efficient preheating. At the same time, the low-amplitude parametric resonance in the case where $m_\chi = m_\phi/2$ allows for efficient preheating at larger values of μ. In this case, the low-k instabilities source χ-particle production over many e-foldings (see Fig. 3), and potentially make it possible for the Universe to fully reheat at much larger values of μ.

However, we find that the presence of a nonzero mass for the axion, $m_\chi \neq 0$, significantly affects the resulting gravitational wave spectra. Using the same techniques as described in Sec. V B, we can compute the resulting gravitational waves the times identified with stars in Fig. 3. These spectra are shown in Fig. 9. Despite the $m_\chi = 0$ and $m_\chi \neq 0$ runs showing similar preheating efficiencies, the amplitude of the gravitational waves produced in the $m_\chi = 0$ case generically exceed those in the $m_\chi \neq 0$, as can be seen in Fig. 10. This effect is pronounced at intermediate values of μ, where the spectra from the massless case exceeds that of the massive case by several orders of magnitude for lower couplings, as we show in Fig. 10. This is particularly relevant for the marginal cases, $\mu \sim 0.18 M_{\rm pl}$.

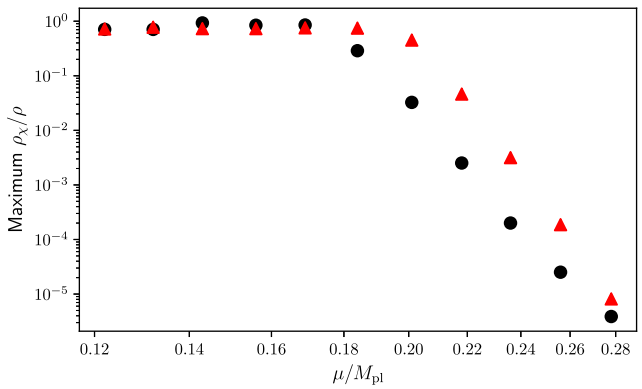

FIG. 8. The preheating efficiency from kinetic preheating with a quadratic potential in the case where χ is massless (black, circles) and massive, $m_\chi = m_\phi/2$, (red triangles). Massive preheating is more efficient here at higher coupling due to the low amplitude resonance identified in the Floquet analysis in Sec. IV A These are the maxima that correspond to the starred points in Fig. 4.

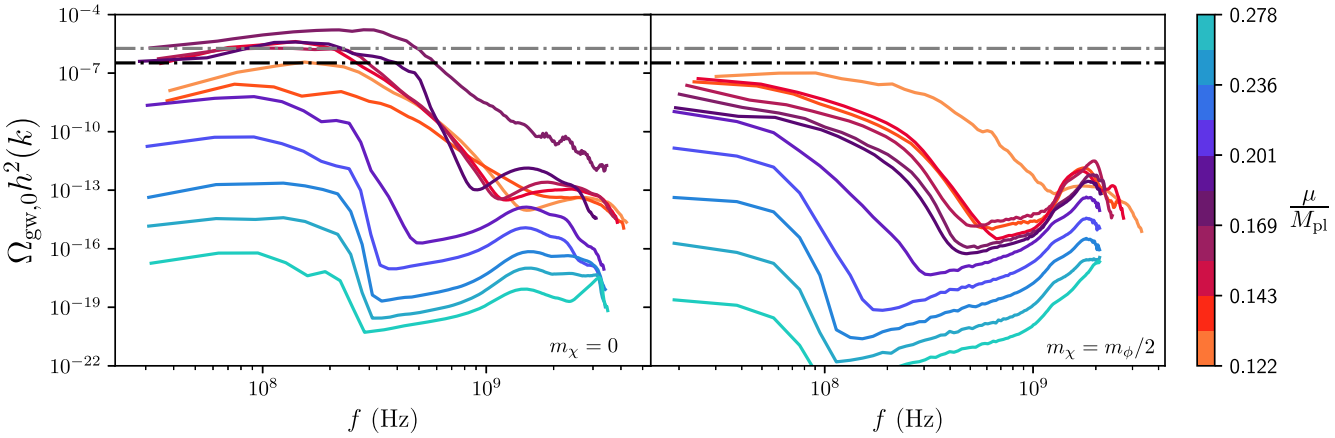

FIG. 9. The gravitational wave spectral energy density from quadratic potential over a range of μ values for a massless χ field (left) and massive χ field, $m_\chi = m_\phi/2$ (right). Simulations that reheat completely and last longer produce stronger gravitational wave backgrounds that are particularly enhanced at the low frequency end of the resolved spectrum. These spectra are evaluated at the starred-locations in Fig. 3.

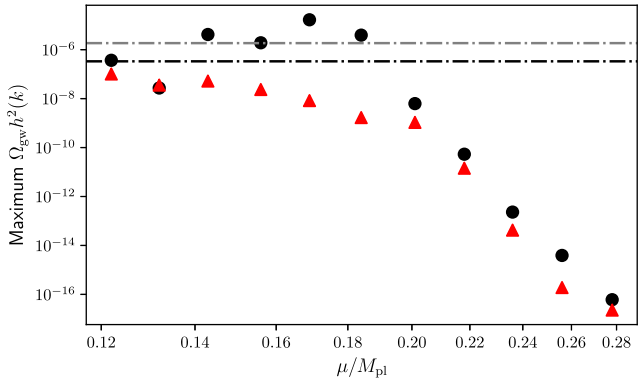

FIG. 10. Maximum spectral energy density in the gravitational wave background as a function of coupling μ. The red triangles show the case where $m_\chi = m_\phi/2$, while the massless case, $m_\chi = 0$, is shown in black circles. Each point represents the maximum value of the gravitational wave spectra presented in Fig. 9.

[1] Alan H. Guth, The inflationary universe: A possible solution to the horizon and flatness problems, Phys. Rev. D **23**, 347 (1981).

[2] Alexei A. Starobinsky, A new type of isotropic cosmological models without singularity, Phys. Lett. **91B**, 99 (1980).

[3] Andrei D. Linde, A new inflationary universe scenario: A possible solution of the horizon, flatness, homogeneity, isotropy and primordial monopole problems, Phys. Lett. **108B**, 389 (1982).

[4] Andreas Albrecht and Paul J. Steinhardt, Cosmology for grand unified theories with radiatively induced symmetry breaking, Phys. Rev. Lett. **48**, 1220 (1982).

[5] Andrei D. Linde, Chaotic inflation, Phys. Lett. **129B**, 177 (1983).

[6] Viatcheslav F. Mukhanov and G. V. Chibisov, Quantum fluctuation and nonsingular universe. (In Russian), Pis'ma Zh. Eksp. Teor. Fiz. **33**, 549 (1981) [JETP Lett. **33**, 532 (1981)].

[7] Alan H. Guth and S. Y. Pi, Fluctuations in the new inflationary universe, Phys. Rev. Lett. **49**, 1110 (1982).

[8] S. W. Hawking, The development of irregularities in a single bubble inflationary universe, Phys. Lett. **115B**, 295 (1982).

[9] James M. Bardeen, Paul J. Steinhardt, and Michael S. Turner, Spontaneous creation of almost scale—free density

perturbations in an inflationary universe, Phys. Rev. D **28**, 679 (1983).
[10] Katherine Freese, Joshua A. Frieman, and Angela V. Olinto, Natural inflation with pseudo—Nambu-Goldstone bosons, Phys. Rev. Lett. **65**, 3233 (1990).
[11] Y. Akrami *et al.* (Planck Collaboration), Planck 2018 results. X. Constraints on inflation, Astron. Astrophys. **641**, A10 (2020).
[12] P. A. R. Ade *et al.* (BICEP, Keck Collaborations), Improved constraints on primordial gravitational waves using Planck, WMAP, and BICEP/Keck observations through the 2018 observing season, Phys. Rev. Lett. **127**, 151301 (2021).
[13] Fedor L. Bezrukov and Mikhail Shaposhnikov, The standard model Higgs boson as the inflaton, Phys. Lett. B **659**, 703 (2008).
[14] Renata Kallosh and Andrei Linde, Non-minimal inflationary attractors, J. Cosmol. Astropart. Phys. 10 (2013) 033.
[15] Jong-Mann Yang, Michael S. Turner, G. Steigman, D. N. Schramm, and Keith A. Olive, Primordial nucleosynthesis: A critical comparison of theory and observation, Astrophys. J. **281**, 493 (1984).
[16] Jennie H. Traschen and Robert H. Brandenberger, Particle production during out-of-equilibrium phase transitions, Phys. Rev. D **42**, 2491 (1990).
[17] Y. Shtanov, Jennie H. Traschen, and Robert H. Brandenberger, Universe reheating after inflation, Phys. Rev. D **51**, 5438 (1995).
[18] Lev Kofman, Andrei D. Linde, and Alexei A. Starobinsky, Reheating after inflation, Phys. Rev. Lett. **73**, 3195 (1994).
[19] Lev Kofman, Andrei D. Linde, and Alexei A. Starobinsky, Towards the theory of reheating after inflation, Phys. Rev. D **56**, 3258 (1997).
[20] S. Y. Khlebnikov and I. I. Tkachev, Relic gravitational waves produced after preheating, Phys. Rev. D **56**, 653 (1997).
[21] Richard Easther and Eugene A. Lim, Stochastic gravitational wave production after inflation, J. Cosmol. Astropart. Phys. 04 (2006) 010.
[22] Richard Easther, John T. Giblin, Jr., and Eugene A. Lim, Gravitational wave production at the end of inflation, Phys. Rev. Lett. **99**, 221301 (2007).
[23] Juan Garcia-Bellido and Daniel G. Figueroa, A stochastic background of gravitational waves from hybrid preheating, Phys. Rev. Lett. **98**, 061302 (2007).
[24] Richard Easther, John T. Giblin, and Eugene A. Lim, Gravitational waves from the end of inflation: Computational strategies, Phys. Rev. D **77**, 103519 (2008).
[25] Jean Francois Dufaux, Amanda Bergman, Gary N. Felder, Lev Kofman, and Jean-Philippe Uzan, Theory and numerics of gravitational waves from preheating after inflation, Phys. Rev. D **76**, 123517 (2007).
[26] Jean-Francois Dufaux, Gary Felder, Lev Kofman, and Olga Navros, Gravity waves from tachyonic preheating after hybrid inflation, J. Cosmol. Astropart. Phys. 03 (2009) 001.
[27] Jean-Francois Dufaux, Daniel G. Figueroa, and Juan Garcia-Bellido, Gravitational waves from Abelian gauge fields and cosmic strings at preheating, Phys. Rev. D **82**, 083518 (2010).
[28] Peter Adshead, John T. Giblin, and Zachary J. Weiner, Gravitational waves from gauge preheating, Phys. Rev. D **98**, 043525 (2018).
[29] Peter Adshead, John T. Giblin, Mauro Pieroni, and Zachary J. Weiner, Constraining axion inflation with gravitational waves from preheating, Phys. Rev. D **101**, 083534 (2020).
[30] Peter Adshead, John T. Giblin, Mauro Pieroni, and Zachary J. Weiner, Constraining axion inflation with gravitational waves across 29 decades in frequency, Phys. Rev. Lett. **124**, 171301 (2020).
[31] Catarina Cosme, Daniel G. Figueroa, and Nicolas Loayza, Gravitational wave production from preheating with trilinear interactions, J. Cosmol. Astropart. Phys. 05 (2023) 023.
[32] Bruce A. Bassett, David I. Kaiser, and Roy Maartens, General relativistic preheating after inflation, Phys. Lett. B **455**, 84 (1999).
[33] Anne M. Green and Karim A. Malik, Primordial black hole production due to preheating, Phys. Rev. D **64**, 021301 (2001).
[34] Karsten Jedamzik, Martin Lemoine, and Jerome Martin, Collapse of small-scale density perturbations during preheating in single field inflation, J. Cosmol. Astropart. Phys. 09 (2010) 034.
[35] Jérôme Martin, Theodoros Papanikolaou, and Vincent Vennin, Primordial black holes from the preheating instability in single-field inflation, J. Cosmol. Astropart. Phys. 01 (2020) 024.
[36] Nathan Musoke, Shaun Hotchkiss, and Richard Easther, Lighting the dark: Evolution of the postinflationary universe, Phys. Rev. Lett. **124**, 061301 (2020).
[37] Pierre Auclair and Vincent Vennin, Primordial black holes from metric preheating: Mass fraction in the excursion-set approach, J. Cosmol. Astropart. Phys. 02 (2021) 038.
[38] Jérôme Martin, Theodoros Papanikolaou, Lucas Pinol, and Vincent Vennin, Metric preheating and radiative decay in single-field inflation, J. Cosmol. Astropart. Phys. 05 (2020) 003.
[39] Benedikt Eggemeier, Bodo Schwabe, Jens C. Niemeyer, and Richard Easther, Gravitational collapse in the postinflationary Universe, Phys. Rev. D **105**, 023516 (2022).
[40] Torsten Bringmann, Pat Scott, and Yashar Akrami, Improved constraints on the primordial power spectrum at small scales from ultracompact minihalos, Phys. Rev. D **85**, 125027 (2012).
[41] Grigor Aslanyan, Layne C. Price, Jenni Adams, Torsten Bringmann, Hamish A. Clark, Richard Easther, Geraint F. Lewis, and Pat Scott, Ultracompact minihalos as probes of inflationary cosmology, Phys. Rev. Lett. **117**, 141102 (2016).
[42] Peter Adshead, John T. Giblin, Timothy R. Scully, and Evangelos I. Sfakianakis, Magnetogenesis from axion inflation, J. Cosmol. Astropart. Phys. 10 (2016) 039.
[43] Mohamed M. Anber and Eray Sabancilar, Hypermagnetic fields and baryon asymmetry from pseudoscalar inflation, Phys. Rev. D **92**, 101501 (2015).
[44] Peter Adshead and Evangelos I. Sfakianakis, Leptogenesis from left-handed neutrino production during axion inflation, Phys. Rev. Lett. **116**, 091301 (2016).
[45] Kohei Kamada and Andrew J. Long, Baryogenesis from decaying magnetic helicity, Phys. Rev. D **94**, 063501 (2016).
[46] R. R. Caldwell and C. Devulder, Axion gauge field inflation and gravitational leptogenesis: A lower bound on *B* modes

from the matter-antimatter asymmetry of the Universe, Phys. Rev. D **97**, 023532 (2018).
[47] Peter Adshead, Andrew J. Long, and Evangelos I. Sfakianakis, Gravitational leptogenesis, reheating, and models of neutrino mass, Phys. Rev. D **97**, 043511 (2018).
[48] Valerie Domcke, Benedict von Harling, Enrico Morgante, and Kyohei Mukaida, Baryogenesis from axion inflation, J. Cosmol. Astropart. Phys. 10 (2019) 032.
[49] Valerie Domcke, Kohei Kamada, Kyohei Mukaida, Kai Schmitz, and Masaki Yamada, Wash-in leptogenesis after axion inflation, J. High Energy Phys. 01 (2023) 053.
[50] Andrei Linde, Dong-Gang Wang, Yvette Welling, Yusuke Yamada, and Ana Achúcarro, Hypernatural inflation, J. Cosmol. Astropart. Phys. 07 (2018) 035.
[51] Matteo Braglia, Dhiraj Kumar Hazra, Fabio Finelli, George F. Smoot, L. Sriramkumar, and Alexei A. Starobinsky, Generating PBHs and small-scale GWs in two-field models of inflation, J. Cosmol. Astropart. Phys. 08 (2020) 001.
[52] Renata Kallosh and Andrei Linde, Dilaton-axion inflation with PBHs and GWs, J. Cosmol. Astropart. Phys. 08 (2022) 037.
[53] Renata Kallosh and Andrei Linde, Polynomial α-attractors, J. Cosmol. Astropart. Phys. 04 (2022) 017.
[54] Peter Adshead, John T. Giblin, and Reid Pfaltzgraff-Carlson, Kinetic preheating after α-attractor inflation, arXiv:2311.17237.
[55] Tomasz Krajewski, Krzysztof Turzyński, and Michał Wieczorek, On preheating in α-attractor models of inflation, Eur. Phys. J. C **79**, 654 (2019).
[56] Oksana Iarygina, Evangelos I. Sfakianakis, Dong-Gang Wang, and Ana Achucarro, Universality and scaling in multi-field α-attractor preheating, J. Cosmol. Astropart. Phys. 06 (2019) 027.
[57] Oksana Iarygina, Evangelos I. Sfakianakis, Dong-Gang Wang, and Ana Achúcarro, Multi-field inflation and preheating in asymmetric α-attractors, arXiv:2005.00528.
[58] Junmei Li, Hongwei Yu, and Puxun Wu, Production of gravitational waves during preheating in α-attractor inflation, Phys. Rev. D **102**, 083522 (2020).
[59] Tomasz Krajewski and Krzysztof Turzyński, (P)reheating and gravitational waves in α-attractor models, J. Cosmol. Astropart. Phys. 10 (2022) 005.
[60] Ana Achúcarro, Renata Kallosh, Andrei Linde, Dong-Gang Wang, and Yvette Welling, Universality of multi-field α-attractors, J. Cosmol. Astropart. Phys. 04 (2018) 028.
[61] Josu C. Aurrekoetxea, Katy Clough, and Francesco Muia, Oscillon formation during inflationary preheating with general relativity, Phys. Rev. D **108**, 023501 (2023).
[62] I. L. Bogolyubsky and V. G. Makhankov, On the pulsed soliton lifetime in two classical relativistic theory models, JETP Lett. **24**, 12 (1976).
[63] I. L. Bogolyubsky and V. G. Makhankov, Dynamics of heavy spherically-symmetric pulsons, Pis'ma Zh. Eksp. Teor. Fiz. **25**, 120 (1977).
[64] Marcelo Gleiser, Pseudostable bubbles, Phys. Rev. D **49**, 2978 (1994).
[65] Edmund J. Copeland, M. Gleiser, and H. R. Muller, Oscillons: Resonant configurations during bubble collapse, Phys. Rev. D **52**, 1920 (1995).
[66] S. Kasuya, M. Kawasaki, and Fuminobu Takahashi, I-balls, Phys. Lett. B **559**, 99 (2003).
[67] Paul M. Saffin and Anders Tranberg, Oscillons and quasi-breathers in $D+1$ dimensions, J. High Energy Phys. 01 (2007) 030.
[68] Mark P. Hertzberg, Quantum radiation of oscillons, Phys. Rev. D **82**, 045022 (2010).
[69] Mustafa A. Amin, Richard Easther, Hal Finkel, Raphael Flauger, and Mark P. Hertzberg, Oscillons after inflation, Phys. Rev. Lett. **108**, 241302 (2012).
[70] Petja Salmi and Mark Hindmarsh, Radiation and relaxation of oscillons, Phys. Rev. D **85**, 085033 (2012).
[71] Stefan Antusch, Francesco Cefala, Sven Krippendorf, Francesco Muia, Stefano Orani, and Fernando Quevedo, Oscillons from string moduli, J. High Energy Phys. 01 (2018) 083.
[72] Fuminori Hasegawa and Jeong-Pyong Hong, Inflaton fragmentation in E models of cosmological α-attractors, Phys. Rev. D **97**, 083514 (2018).
[73] Marcelo Gleiser and Max Krackow, Resonant configurations in scalar field theories: Can some oscillons live forever?, Phys. Rev. D **100**, 116005 (2019).
[74] Stefan Antusch, Francesco Cefalà, and Francisco Torrentí, Properties of oscillons in hilltop potentials: Energies, shapes, and lifetimes, J. Cosmol. Astropart. Phys. 10 (2019) 002.
[75] Masahiro Ibe, Masahiro Kawasaki, Wakutaka Nakano, and Eisuke Sonomoto, Decay of I-ball/oscillon in classical field theory, J. High Energy Phys. 04 (2019) 030.
[76] Hong-Yi Zhang, Mustafa A. Amin, Edmund J. Copeland, Paul M. Saffin, and Kaloian D. Lozanov, Classical decay rates of oscillons, J. Cosmol. Astropart. Phys. 07 (2020) 055.
[77] Fabio van Dissel, Oriol Pujolas, and Evangelos I. Sfakianakis, Oscillon spectroscopy, J. High Energy Phys. 07 (2023) 194.
[78] Stefan Antusch, Francesco Cefala, and Stefano Orani, Gravitational waves from oscillons after inflation, Phys. Rev. Lett. **118**, 011303 (2017); **120**, 219901(E) (2018).
[79] Mustafa A. Amin, Jonathan Braden, Edmund J. Copeland, John T. Giblin, Christian Solorio, Zachary J. Weiner, and Shuang-Yong Zhou, Gravitational waves from asymmetric oscillon dynamics?, Phys. Rev. D **98**, 024040 (2018).
[80] Peter Adshead, Kaloian D. Lozanov, and Zachary J. Weiner, Dark photon dark matter from an oscillating dilaton, Phys. Rev. D **107**, 083519 (2023).
[81] Hillary L. Child, John T. Giblin, Jr., Raquel H. Ribeiro, and David Seery, Preheating with non-minimal kinetic terms, Phys. Rev. Lett. **111**, 051301 (2013).
[82] J. Tate Deskins, John T. Giblin, and Robert R. Caldwell, Gauge field preheating at the end of inflation, Phys. Rev. D **88**, 063530 (2013).
[83] Peter Adshead, John T. Giblin, and Zachary J. Weiner, Non-Abelian gauge preheating, Phys. Rev. D **96**, 123512 (2017).
[84] Charles W. Misner, K. S. Thorne, and J. A. Wheeler, *Gravitation* (W. H. Freeman, San Francisco, 1973).
[85] John T. Giblin and Eric Thrane, Estimates of maximum energy density of cosmological gravitational-wave backgrounds, Phys. Rev. D **90**, 107502 (2014).

[86] N. Aghanim *et al.* (Planck Collaboration), Planck 2018 results. VI. Cosmological parameters, Astron. Astrophys. **641**, A6 (2020); **652**, C4(E) (2021).
[87] Kevork Abazajian *et al.*, CMB-S4 science case, reference design, and project plan, arXiv:1907.04473.
[88] E. Grohs, G. M. Fuller, C. T. Kishimoto, M. W. Paris, and A. Vlasenko, Neutrino energy transport in weak decoupling and big bang nucleosynthesis, Phys. Rev. D **93**, 083522 (2016).
[89] Pablo F. de Salas and Sergio Pastor, Relic neutrino decoupling with flavour oscillations revisited, J. Cosmol. Astropart. Phys. 07 (2016) 051.
[90] Kensuke Akita and Masahide Yamaguchi, A precision calculation of relic neutrino decoupling, J. Cosmol. Astropart. Phys. 08 (2020) 012.
[91] Brian D. Fields, Keith A. Olive, Tsung-Han Yeh, and Charles Young, Big-bang nucleosynthesis after Planck, J. Cosmol. Astropart. Phys. 03 (2020) 010; 11 (2020) E02.
[92] J. Aasi *et al.* (LIGO Scientific Collaboration), Advanced LIGO, Classical Quantum Gravity **32**, 074001 (2015).
[93] Pau Amaro-Seoane *et al.* (LISA Collaboration), Laser interferometer space antenna, arXiv:1702.00786.
[94] Benjamin P Abbott *et al.* (LIGO Scientific Collaboration), Exploring the sensitivity of next generation gravitational wave detectors, Classical Quantum Gravity **34**, 044001 (2017).
[95] S. Hild *et al.*, Sensitivity studies for third-generation gravitational wave observatories, Classical Quantum Gravity **28**, 094013 (2011).
[96] John T. Giblin and Avery J. Tishue, Preheating in full general relativity, Phys. Rev. D **100**, 063543 (2019).
[97] Peter Adshead, John T. Giblin, Ryn Grutkoski, and Zachary J. Weiner, Gauge preheating with full general relativity, arXiv:2311.01504.
[98] Peter Adshead, John T. Giblin, Jr., and Avery Tishue, Kinetic preheating with full general relativity (to be published).
[99] Ohio Supercomputer Center, Ohio supercomputer center (1987), http://osc.edu/ark:/19495/f5s1ph73.